ACS OMEGA

http://pubs.acs.org/journal/acsodf

Article

3D Quantitative Prediction of the Groundwater Potential Area—A Case Study of a Simple Geological Structure Aquifer

Liyao Li, Fei Xia,* Jinhui Liu, Kai Zang, Chao Liu, Jiuchuan Wei, and Longlong Liu

Cite This: *ACS Omega* 2022, 7, 18004−18016

Read Online

ACCESS | Metrics & More | Article Recommendations

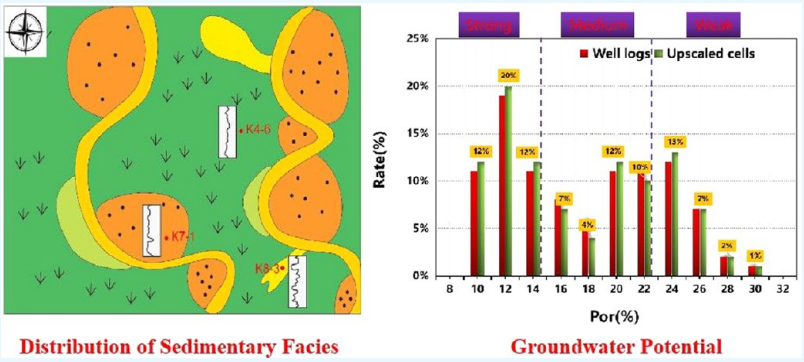

ABSTRACT: The Ordos Basin is a sedimentary basin located in Inner Mongolia, China, where coal and uranium coexist. Water inrush disasters have always been one of the main disasters that threaten the safety of coal mine production, and thus, the study and division of groundwater potential regions are of great significance for the prevention of water inrush disasters and in situ leaching of sandstone-type uranium ore. A new method combining truncated Gaussian simulation and sedimentary facies control was established to predict the groundwater potential area. Taking a typical aquifer, the Zhiluo Formation, as an example, based on high-resolution sequence stratigraphy, geophysics, sedimentary geology, and geostatistical theory, the plane distribution of sand bodies was predicted. Furthermore, the relationship between rock porosity and electricity porosity was established to calculate the regional porosity. Combined with truncated Gaussian simulation and facies-controlled modeling methods, a facies-controlled heterogeneous property model was established to analyze the heterogeneous effective porosity of the aquifer in the study area. Groundwater potential areas were quantitatively evaluated by 3D modeling analysis. The results of the evaluated model were verified by actual data and provide a geological guarantee for the accurate mining of deep coal and uranium ore. A 3D distributed model of chemical elements, which is meaningful for in situ leaching uranium mining, is expected in future research.

1. INTRODUCTION

There are relatively rich coal resources in China. In particular, the coalfields in the Ordos Basin exhibit excellent occurrence conditions and play an important role in the development of coal energy in China.[1,2] Unfortunately, groundwater inrush disasters in coal mines are frequent occurrences.[2,5] In addition, many sandstone-type uranium ore deposits are associated with coal in the Ordos Basin because of the coal reducibility. Coal and uranium resources often coexist in the Ordos Basin.

The Early and Middle Jurassic coal-bearing strata in the Ordos Basin were deposited in an inland lake basin environment with well-developed fluvial and lacustrine delta sediments. The distribution of sand bodies was complex, the sand bodies were spatially superimposed on each other, and the sedimentary facies transition was rapid. With the large-scale mining of coal, water inrush accidents in coal mines frequently occur.[4] The fundamental reason for these accidents is poor understanding of the reserved capacity and distributed rule of aquifers.[2,5] In addition, the mineralization of sandstone-type uranium deposits is also controlled by the distribution of aquifers.,[6] The perspective of sedimentary genesis can well predict the spatial distribution of aquifers and explain the hydrodynamic properties of aquifers; thus, sedimentology studies can provide geological guarantees for the safe production of coal mine and the in situ leaching of sandstone-type uranium.[3]

At present, prediction studies of the groundwater potential area and groundwater inrush in coal mines can be divided into three categories. The first class of approaches are based on unit

Received: March 8, 2022
Accepted: May 5, 2022
Published: May 17, 2022

inflow data, fault density, and other groundwater potential control factors. Yin used a GIS-based model to integrate these correlative water potential factors.[1] Wu proposed a vulnerability index coupling the analytic hierarchy process (AHP) with a geographic information system (GIS).[7] A synthetic method was developed to evaluate the groundwater potential of a confined aquifer overlying a mining area using the improved set pair analysis (ISPA) theory.[2]

Other approaches involve evaluating the groundwater potential area through geophysical detection methods, such as the direct current method and transient electromagnetic method. Gao used 2D electrical resistivity tomography (ERT) by laying electrodes and cables in two adjacent roadways and using an equatorial dipole device to detect the groundwater potential internal working face.[8] Shi developed equipment and corresponding data processing software to collect 3D data volume for a working face, and 3D imaging technology was combined to realize the 3D detection of a groundwater potential working face before mining.[2] The third approach is focused on water inrush risk caused by overburden aquifer destruction. The experimental, theoretical, and in situ methods were used to verify the protection of the overburden aquifer by gangue backfilling mining.[24] Ma analyzed the characteristics of water-sediment flow in fractures by computational fluid dynamics, which are expected to determine the mechanism water-sediment inrush.[26] These methods have achieved certain results, but due to the multiple interpretations of geophysical data and the limitations of hydrogeological data, such as few hydrogeological holes and partial experiments, errors in prediction results arise, and neither method analyzes the groundwater potential of a unconsolidated aquifer itself.

Guided by the concept of "groundwater controlled by depositional architecture",[7] this manuscript takes the Zhiluo Formation of the Ordos Basin as an example. According to logging, core analysis, and laboratory experiments, the distribution of sedimentary facies belts in different stratigraphic frameworks was predicted. Based on overpressure porosity test data and logging data, the regional porosities of different layers were measured, and the truncated Gaussian simulation method was used to discretize the measured porosities controlled by sedimentary facies. Then a facies-controlled heterogeneous groundwater potential model was established to predict the accumulation area of groundwater.

2. METHODS

2.1. Analysis of Sedimentary Facies in the Sequence Stratigraphic Framework. The spatial contact relation of sand bodies is affected by sedimentary facies. The analysis of sedimentary facies starts by identifying facies markers, such as the color of sedimentary rock, particle size, and sedimentary structure. Based on the sedimentary analysis results, the distribution system of sedimentary microfacies is established based on the theory of facies differentiation and facies contact.

2.2. Porosity Measurement Based on Lithoelectric Regression. The porosity of sandstone is an important index for the quantitative evaluation of pore aquifers.[9] A change in effective pressure in the rock matrix causes a change in the porosity in the rock; therefore, the confining pressure of rock samples was increased in a laboratory to simulate authentic strata overlying pressure. The first step of the test procedure is production of standard rock samples; second, the samples are put into the core gripper and pressure is applied to the core, with the pressures being dependent on burial depth; and third, the measurement medium is nitrogen, which is diffused into the core. Boyle's law was used in the measurement, and the nitrogen volume was measured by change of pressure. Finally, the effective pore volume was obtained by nitrogen volume.

Due to limitations on the number of samples tested, the porosity distribution law cannot be comprehensively reflected. Thus, acoustic time (AC) logging and laboratory experiments were carried out for regression analysis, the corresponding lithoelectric relationship was established, and the porosities of untested strata and regions were calculated to evaluate the water storage capacity of aquifers.

2.3. Establishment of the Facies-Controlled Heterogeneous Porosity Model. Facies-control modeling is based on the time and space distribution characteristics of sedimentary facies to restrict reservoir stochastic modeling. The core procedure starts with a sedimentogenesis analysis to guide the modeling process, which involves using the plane and vertical evolution of sedimentary facies to restrict 3D modeling results.

The thickness and porosity of an aquifer are important indexes that affect the groundwater potential of a unconsolidated aquifer. By establishing a facies-controlled porosity model, the distributions of sedimentary facies and porosity parameters are combined to depict the groundwater potential areas in the target strata.

2.3.1. Truncated Gaussian Simulation. Truncated Gaussian simulation belongs to the discrete random model, which is used to study discrete or type variables.[10] The simulation process establishes the 3D distribution of variables by truncating the 3D continuous variables through truncating rules.[20] The truncating rule is determined according to different sedimentary facies; that is, the same truncating rule is set for the same sedimentary facies. The specific approach is as follows:

Suppose "n" kinds of sedimentary facies can be described by the indicator function of each sedimentary facies. For the "i" sedimentary facies, its indicator value can be defined by Gaussian random function $Y(x)$:

$$I(a_{i-1} < Y(x) \le a_i) = \begin{cases} 1 & Y(x) \in (a_{i-1}, a_i) \\ 0 & \text{other} \end{cases}$$

Thus, point x belongs to i sedimentary facies if and only if $Y(x) \in (a_{i-1}, a_i)$, and a_i is the truncated value, which is used to truncate the 3D continuous variables.

The establishment procedure of 3D continuous variables (Gaussian simulation procedure) was common and fixed based on the specific procedure cited by Lee and Verly.[11,12] The truncated Gaussian simulation was written into Petrel software to command calls at any time.

2.3.2. Facies-Controlled Porosity Modeling. The truncated Gaussian simulation method is a purely mathematical simulation method, which is a random simulation method that cannot normally be combined with geological understanding. Therefore, it is necessary to apply a variation function to control the simulation results to have the simulation results controlled by geological understanding (sedimentary facies).

Different sedimentary facies are controlled not only by different truncation rules but also by the variation function of different parameters. The variation function changes with lag distance u, and the change features show various spatial variation properties of regional variables. The spherical variation function was applied in this model. Compared to

https://doi.org/10.1021/acsomega.2c01387
ACS Omega 2022, 7, 18004−18016

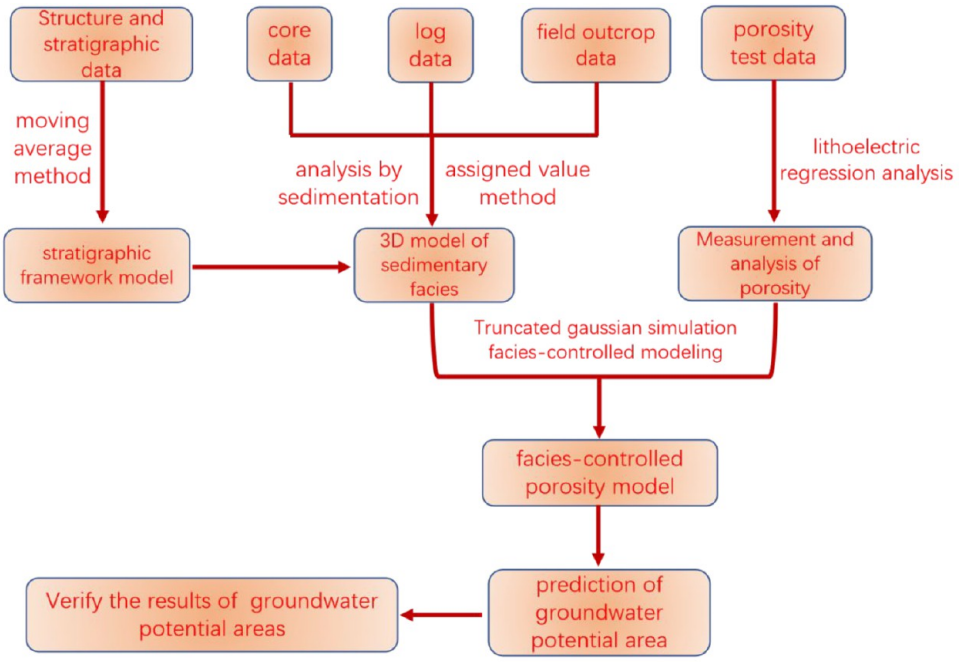

Figure 1. Flowchart of the 3D spatial prediction of the groundwater potential area under facies control.

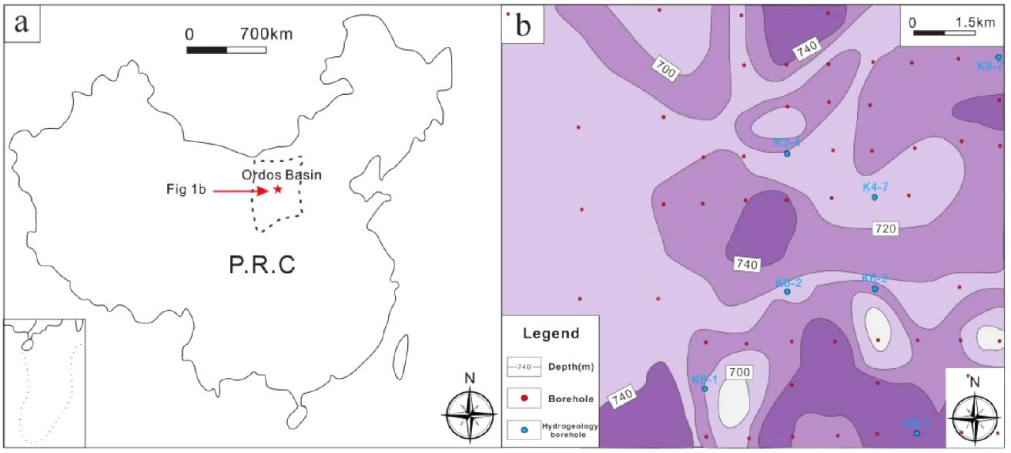

Figure 2. (a) Location map of the study area; (b) top surface structure map of the study area.

those of other variation functions, the control data abilities of the spherical model are more accurate, and its specific expression is outlined as follows:

$$r(h) = \begin{cases} c \times \left(1.5\frac{h}{a} - 0.5\frac{h^3}{a^3}\right), & h \le a \\ c, & h > a \end{cases} \quad (1)$$

Here, a is the range of the variation function, meaning the spatial correlation range of regional variables; h is the lag distance, which is the independent variable of the variation function. c is a partial sill, which represents the total variability level of the variable in space. In practical modeling applications, the parameters of the variation function were adjusted according to the difference in geological understanding so that the variation function could reflect actual geological conditions as comprehensively as possible.

Figure 1 shows the construction process of the sedimentary facies control model of the groundwater potential area. The digitized top and bottom surface and individual layer data collected from each bore hole are used to establish a sequence stratigraphic framework model. The core, logging, and outcrop data are the basic data for sedimentary facies analysis, and the distribution of sedimentary facies is determined by the results of sedimentary analysis. Combining acoustic time logging with petrophysics experimentation, the porosity data of the target area were calculated by the lithoelectric regression formula, and the discrete results controlled by the sedimentary facies were discretized by truncated Gaussian simulation. Finally, the 3D spatial prediction model of groundwater potential areas was established.

3. RESULT: A CASE STUDY

3.1. Geology and Hydrogeology Settings. The study area is located in the middle of the Ordos Basin in northern China (Figure 2a). The geological and hydrogeological features of this area are typical: the terrain is flat, and there are no faults in the main mining area (Figure 2b). According to

https://doi.org/10.1021/acsomega.2c01387
ACS Omega 2022, 7, 18004−18016

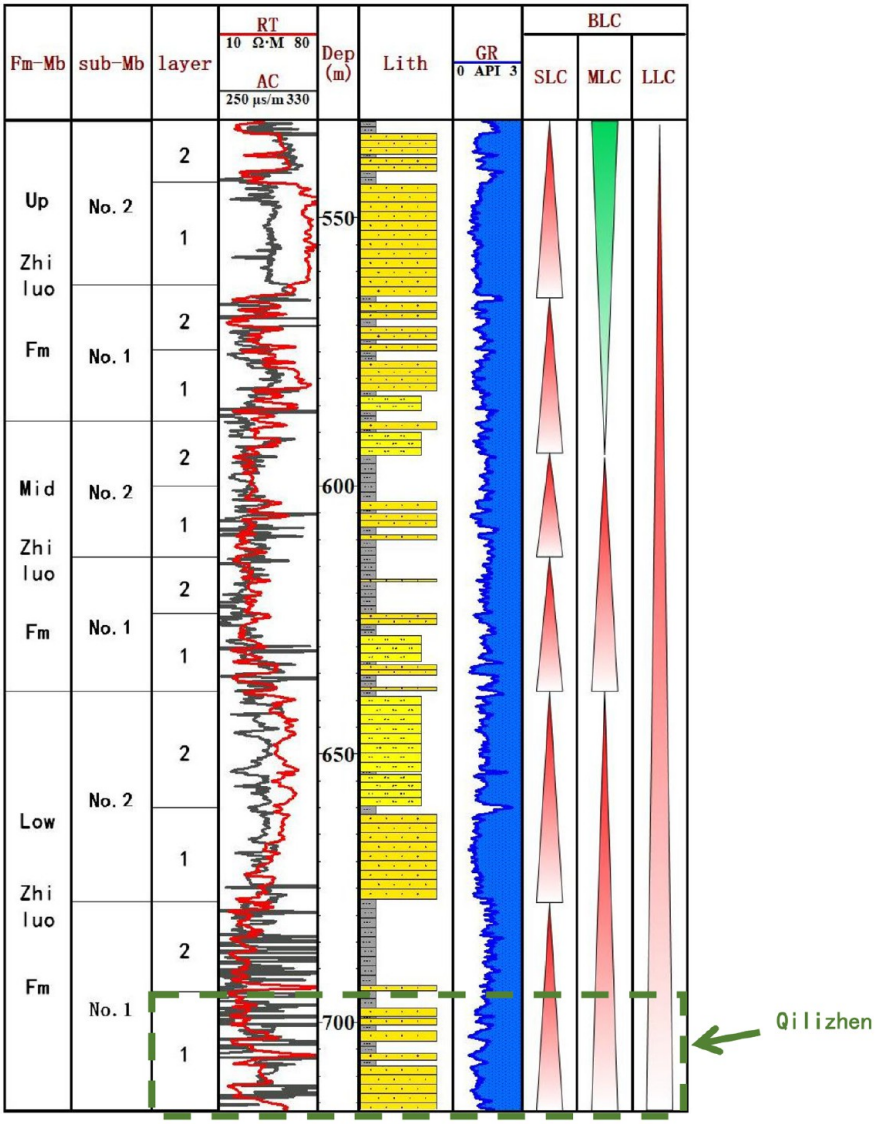

Figure 3. Sequence stratigraphy and lithology division of the Zhiluo Formation (Fm: Formation; Mb: Member; Dep: Depth; Lith: lithology; BLC: base-level cycle; SSC: short-level cycle; MSC: middle-level cycle; LLC: long-level cycle).

core observations and outcrop observations of primary research,[13] there is also no obvious primary fracture in the target area. The coal-bearing strata of this target area are located in the middle Jurassic Yan 'an Formation, and the overlying Zhiluo Formation, providing the direct water filling of coal, has developed a set of pore confined aquifers interlaced with sand and mud (Figure 3).

According to previous research results, the Zhiluo Formation exhibits a long-level cycle (LLC). Three short-level cycles, corresponding to the upper, middle, and lower members of the Zhiluo Formation, were identified in this formation. The three members were further divided into two short-level cycles corresponding to two submembers. In the study area, the upper member of the Zhiluo Formation is approximately 55−75 m thick, and it has relatively thick sandstone but poor continuity. The middle member of the Zhiluo Formation is approximately 45−70 m thick with relatively thin sandstone. The lower member of the Zhiluo Formation is approximately 60−90 m thick, and the "Qilizhen Sandstone" at the bottom of this member is a regional marker with good continuity in the Ordos Basin (Figure 3).

3.2. Sedimentary Characteristics and Facies Distribution of the Zhiluo Formation in the Study Area. The sedimentary system of the study area is controlled by the sedimentary environment of the Ordos Basin according to previous identifications of sedimentary systems.[13,19] Meandering rivers, braided river deltas and braided river sedimentary systems are developed in the upper, middle, and lower members of the Zhiluo Formation, respectively. This manuscript focuses on the classification and identification of sedimentary microfacies in different sedimentary systems based on previous research and finally establishes the distribution system of sedimentary microfacies for the study area on the basis of the theory of microfacies differentiation and microfacies contact.

Based on logging facies and core analysis, the meandering river sedimentary system of the upper Zhiluo Formation is taken as an example (Figure 4). The lithology of the meandering river channel deposition is mainly composed of medium coarse sandstone, and logging at the center of the channel corresponds to the logging characteristics of a smooth box, reflecting a strong hydrodynamic force and stable water

https://doi.org/10.1021/acsomega.2c01387
ACS Omega 2022, 7, 18004−18016

log characteristics		log figure (GR)	sandstone profile	core photo	description	sedimentary facies
electrofacies	smooth box type				medium-coarse sandstone located in river center	channel
	gear box type				medium-coarse sandstone mud intercalation appeared along the river	
	bell or box type				medium-coarse sandstone located in the convex bank of channel normally	point bar
	finger type				Sand mud interbedded located in the concave bank of channel normally	flood fan natural levee
	flat or low amplitude gear				siltite or mud	flood basin

Figure 4. Identification of meandering river and rock facies in the upper member of the Zhiluo Formation.

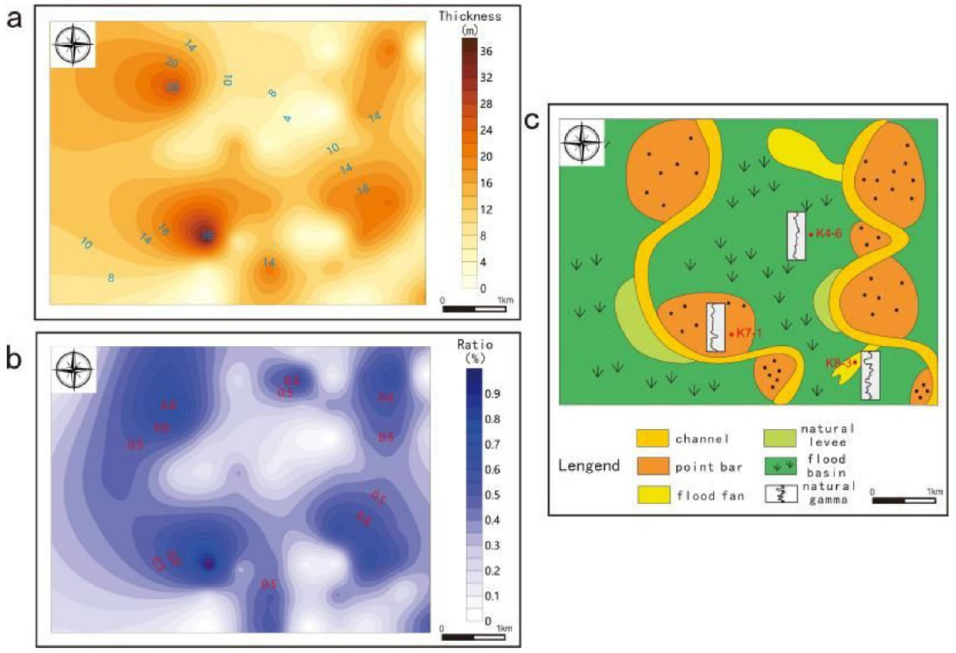

Figure 5. Distribution of sand bodies in the upper member No. 2 submember of the Zhiluo Formation (J_2z_{32}): (a) thickness distribution of two submembers; (b) ratio of sandstone and stratum; (c) distribution of sedimentary facies.

flow. The logging of the channel edge is characteristic of the toothed box, which reflects a strong hydrodynamic force and unstable water flow. Some mud interlayers often occur in channel edge deposition. The section shape of the channel deposit is generally a typical lenticular shape with wide upper and narrow lower areas. The point bar sedimentary microfacies form the underwater deposit located on the convex bank of a curved riverbed; however, it often becomes a relatively large part of the riverbed during the drought period. The logging curve of the point bar is characterized by the bell box type, thick sandstone, and plate and trough cross-stratification. The profile of sandstone is elliptical lenticular in the point bar sediment. After a river burst, a large volume of clastics carried by water flow forms a fan topography at the break. These kinds of deposits are usually composed of thin sandstones with sand and mud interbeds, and logging characteristics are always of the finger or gear type. The natural levee is located at the edge of the meandering riverbed, which is mainly composed of fine sandstone, siltstone, and mudstone. The particle size of the natural levee is thinner than that of the flood fan, but the logging characteristics are similar to those of the flood fan. Located outside the natural levee, the flood basin is the product of clastic vertical accretion on the broad plain outside the riverbed, also known as an alluvial flat deposit. The lithologic structure of flood fans is simple, mainly comprising mudstone and argillaceous siltstone; sandstone levels are low; and the logging curve is generally relatively straight (Figure 4). According to the characteristics of the sedimentary system, the

https://doi.org/10.1021/acsomega.2c01387
ACS Omega 2022, 7, 18004−18016

sedimentary microfacies of the estuary dam, underwater distributary channel, and sand sheet were identified in the middle member of the Zhiluo Formation; the braided channel, batture, and channel overflow of the lower Zhiluo Formation were identified by logging and core analysis.

Combined with logging and core data,[14] the characteristics of sedimentary microfacies in the corresponding layer of each borehole were analyzed, and the plane distribution system of sedimentary microfacies in the main mining area was established. Parts a and b of Figure 5 show the plane layout of the sandstone and the sand and stratum ratio of layer J_2z_{32}. The sandstone displays poor continuity on the plane, and areas of thicker sandstone develop locally. The natural γ of borehole k7-1 presents a smooth box type and toothed box type, and the point bar deposit was drilled in this layer (Figure 5c). The natural γ of borehole k4-6 has a low-amplitude toothed shape, and the flood basin deposit was drilled in this layer (Figure 5c).

3.3. Porosity Measurement of the Study Area. *3.3.1. Overpressure Porosity Experiment of the Target Area.* The burial depth of the Zhiluo Formation is between 500 and 690 m. To simulate the rock porosity change at different depths, an indoor experiment based on different overpressures was carried out. The overpressures of the upper, middle, and lower members are 7.5, 9.5, and 11.5 MPa, respectively, based on burial depth. The specify test procedures are as follows:

The J_2z_1 porosity of the 36 samples ranged from 20.14% to 25.74% with an average of 22.82%; the porosity of J_2z_2 ranged from 10.75% to 25.41% with an average of 18.32%; and the porosity of J_2z_3 ranged from 12.24% to 27.61% with an average of 20.82%.

3.3.2. Measurement and Calculation of the Effective Porosity of the Target Area. According to the results of the overpressure porosity test of the Zhiluo Formation and the mean value of acoustic time (AC), the lithoelectric relationship of the Zhiluo Formation in the target area was established (Figure 6). In formula $y = 0.0485x + 9.579$, the effective

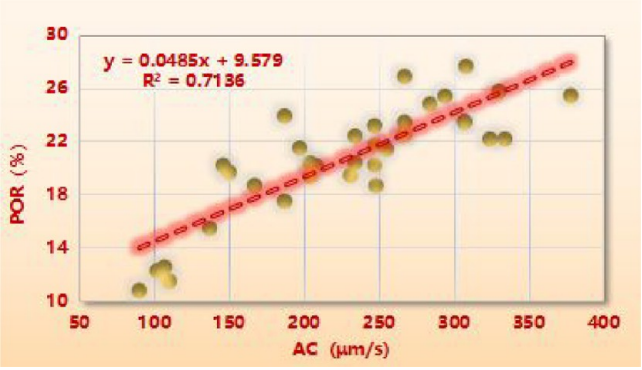

Figure 6. Lithoelectric relationship of the Zhiluo Formation.

porosity value (y) of the untested layer was obtained according to the mean value of AC (x) in the same layer. Figure 6 shows the measured porosities in borehole k3-8. The porosities were measured by logging according to the regression formula and multiplied by the corresponding mud correction coefficient. Referencing some correction coefficients around the study area, the mud stratum takes a value of 0.16, sand-mud interbedding takes a value of 0.6, and the sandstone stratum takes a value of 1.[15] The AC value of sandstone is relatively stable, but the AC value of sand-mud interbedding fluctuates greatly (Figure 7).

3.3.3. Statistical Analysis of Effective Porosity. To clarify the relationship between effective porosity and sedimentary facies, the effective porosity data corresponding to each borehole and layer in the study area were divided and statistically analyzed (Table 1). The riverbed clastic lag deposit, which sedimented in a high hydrodynamic environment, shows a higher level of effective porosity than the riverbed clastic overflow deposit.

3.4. Establishment of the Facies-Controlled Heterogeneous Porosity Model. *3.4.1. 3D Stratigraphic Framework Model of the Study Area.* The establishment of a stratigraphic framework model, which was here used to represent the regional structure, is the first step of the porosity model.[16] There is no fault in the study area, so the fault model is not involved in the framework model. The modeling step is outlined as follows:

First, the study area should be settled and gridded (Figure 8a). The size of the grid is determined by the accuracy of the model. The smaller the grid is, the more accurate the model is. Then the hierarchical data (Figure 8b) are imported, and the sliding average method is applied to generate the stratigraphic interface model (Figure 8c). Finally, based on the establishment of each stratigraphic interface model, the 3D stratigraphic framework model of each layer is built (Figure 8d). Each zone represents the stratigraphic framework of different layers (Figure 8e).

3.4.2. Facies-Controlled Porosity Model. The second step of facies-controlled porosity model establishment is to establish a depositional microfacies model of the study area. According to the analytical results of sediments in the Zhiluo Formation, braided rivers, braided river deltas and meandering river deposit systems developed in the study area. According to borehole and logging identification results, these three depositional systems contain many sedimentary microfacies. The results of depositional facies identification and distribution were directly input into the model using the assigned value method. The assigned value method is a deterministic modeling method, which means that the final modeling result agrees with geological understanding. Taking the meandering river deposition of J_2z_{31-1} as an example, a 2D sedimentary microfacies map was established based on the analysis results of sedimentary characteristics and facies distribution (Figure 9a). Then, a depositional microfacies model of J_2z_{31-1} was established (Figure 9b). According to field outcrop observations for the Ordos Basin channel, point bar and flood fan sediments present a lens-type profile (Figure 9c).[13,21]

The next step of porosity model establishment involves importing the calculated results of the effective porosity data into the model. The facies-controlled method was applied through the adjustment of variogram parameters, which include the range and azimuth. These parameters were adjusted according to the different distributed characteristics of sedimentary microfacies. At the same time, other geological factors, such as sedimentary microfacies boundaries, limited the layout of the facies-controlled porosity.

The major range indicates the influencing sphere of the major source material direction, while the minor range indicates the influencing sphere of the vertical material source direction. The adjustment and modification of variogram parameters were under the control of meandering river deposition (Figure 10 left); for instance, the proportion of

https://doi.org/10.1021/acsomega.2c01387
ACS Omega 2022, 7, 18004−18016

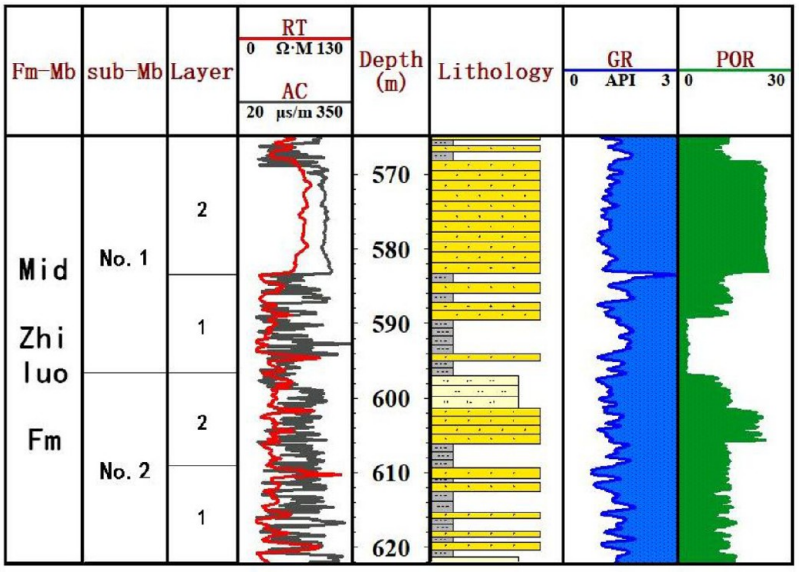

Figure 7. Logging porosity measurement results for the study area.

Table 1. Porosity Distribution of Different Sedimentary Microfacies

		porosity (%)	
sedimentary type	sedimentary facies	range	mean
Riverbed clastic lag deposit	channel	8.3–26.6	20.62
	point bar	10.1–29.7	23.94
	batture	15.4–27.8	20.54
	estuary dam	13.2–22.8	18.14
Riverbed clastic overflow deposit	sand sheet	11.7–17.6	14.42
	natural levee	12.7–15.2	13.14
	interdistributary bay	13.9–16.7	14.51
	flood plain	8.7–12.4	10.57

extended distance in the major and minor directions was 1.25:1 in the point bar deposit, while the proportion of extended distance in the major and minor directions was 2.26:1 in the main course deposit (Table 2). The vertical range, affected by the thickness of sandstones, is the vertical influence sphere of the imported data; for example, the vertical range parameters of flood plain deposits are lower than those of point bar deposits. The azimuth, in terms of angles, controls the direction of the material source and flow. For example, in J_2z_{31-1}, most angles range from 320°–340°, which means that the direction of the material source runs from northeast (Table 2).

Figure 10 presents an example of meandering river deposition in small layer $J_2z_{31}{}^{-1}$ in the study area. A spherical variogram model was selected due to its preferred fitting precision and the actual data volume.[17] By adjusting the shape of the search cone and modifying the parameters of the variogram, the trend of fitting variogram data is according to the actual semivariance data, which means that the variogram is credible (Figure 10, right).

Finally, the 3D visual effective porosity model was established. Figure 11 shows the sedimentary microfacies model and corresponding porosity model. Because of microfacies control, these channel and dam deposits have the best porosity in the 3D model, and the plane distribution of porosity is controlled by the sedimentary facies; sandstones deposited in environments, such as sand sheets, flood fans, and natural levees, have moderate porosity in the 3D model; flood plain deposits have the worst porosity.

3.4.3. Prediction of the Grade of the Heterogeneous Groundwater Potential Area. When applied to the porous aquifer in the study area, the established 3D model can serve as a main tool to predict the groundwater potential area in the study area. A total of 816,900 grids were generated in the 3D model, indicating that there are 816,900 porosity values in the 3D model. The minimum, maximum, and median porosity values are 8.29%, 28.73%, and 16.12%, respectively. Figure 12 shows a histogram of porosity generated in the 3D porosity model of the study area. According to the principle of dispersed porosity data and the natural split point classification rule, threshold values of 14% and 22% are determined.[18] As a result, the groundwater potential in the study area was divided into three grades: weak, moderate, and strong.

3.5. Validation, Discussion, And Expectations.

3.5.1. Validation by Hydrogeological Observation Data. To verify the predicted reliability of the 3D heterogeneous groundwater potential model, long-term hydrogeological observation hole data were collected from the coal mine, and field test data were used to validate the groundwater potential classification results in different strata sequences. The pumping horizon of the observation hole is mainly concentrated in the Zhiluo Formation (J_2z), which is the main aquifer of the coal seam roof, and part of it is in the Yan 'an Formation. The steady flow method was used in the pumping test, which is a continuous process without interruption as far as possible during the test period. In order to reduce error, the method of three times lowering depth was used for testing. Hydrochemical tests were used to analyze the groundwater; here, the pH value of this area is 7.6, the salinity is 1918.87 mg/L, and the type of groundwater is SO_4^{2-}–Na^+·Ca^{2+}.

Referring to the classification criteria of hydrogeological types cited in "Stipulation of Groundwater Prevention and Control in Coal Mines", an industry reference standard for coalfield hydrogeology in China, seven hydrogeological observation hole data were used for comparisons with the predicted result of the 3D porosity model (Figure 2). There

https://doi.org/10.1021/acsomega.2c01387
ACS Omega 2022, 7, 18004–18016

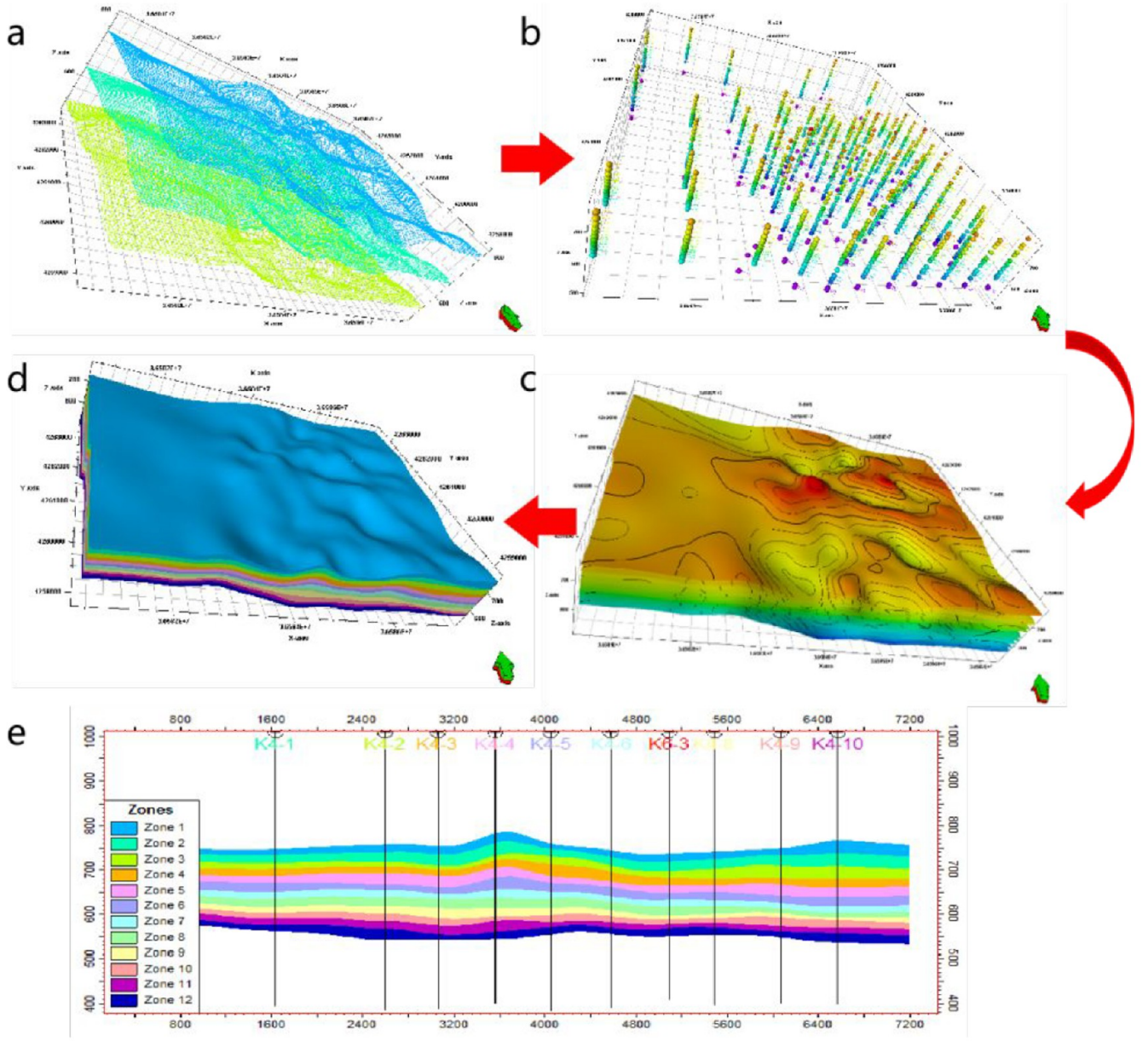

Figure 8. Stratigraphic framework model of the study area: (a) grid of the model; (b) imported hierarchical data; (c) stratigraphic interface model; (d) 3D stratigraphic framework model; (e) stratigraphic framework of different layers.

are 15 different layers which correspond to 12 different sedimentary environment in the seven hydrogeological observation holes (Table 3); all of the holes were well-proportioned and distributed in different parts of the target areas. The results show that deposits such as channel and dam deposits show high unit water inflow and relatively strong groundwater potential, reaching the medium-strong groundwater potential grade; deposits such as flood plains and natural levee deposits indicate less unit water inflow and a weak groundwater potential grade. The specific yield (q), sedimentary microfacies, and results of the 3D facies-controlled porosity model are well correlated, and the predicted results are also consistent with the actual data (Table 3).

3.5.2. Discussion of the 3D Groundwater Potential Area Model. Compared to the 2D groundwater potential method used in previous research,[1] 3D-visualized groundwater potential prediction can more directly depict the spatial form of aquifers. 3D visualized prediction can also quantitatively represent the groundwater potential of aquifers and connectivity between different aquifers in 3D space.[22,23] The 3D groundwater potential model can be used to slice profiles and divide arbitrary sections into different layers and directions, which is beneficial for mine hydrogeologists to prevent and predict mine water disasters. Sedimentary geological bodies were deposited in different geological periods; thus, the distributed rule of sand bodies in each period differs due to provenance supply and other reasons, leading to the complex heterogeneity of sedimentary strata. If the modeling target layer is simulated as a whole, traditional "one-step modeling" is relatively simple, and the hardware requirements are low. However, this method leads to the model not objectively reflecting geological reality. Therefore, the modeling step after stratigraphic division can reduce the error caused by modeling as a whole target layer.

https://doi.org/10.1021/acsomega.2c01387
ACS Omega 2022, 7, 18004−18016

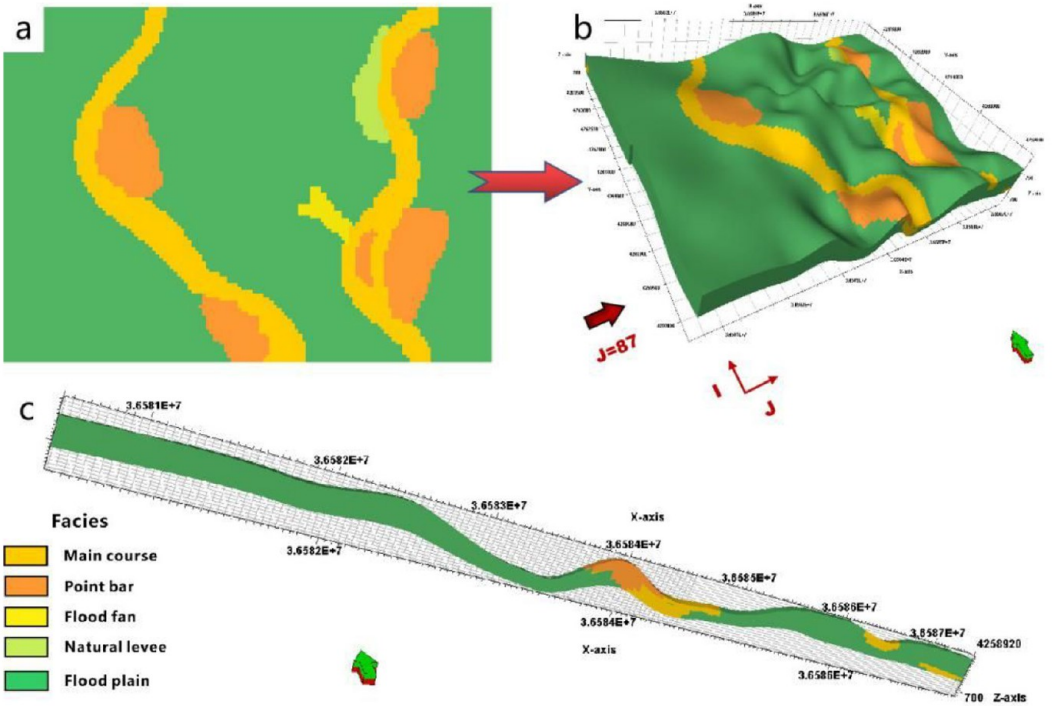

Figure 9. Sedimentary microfacies model establishment (a) 2D sedimentary microfacies distribution; (b) 3D sedimentary microfacies model; (c) 3D cross-section sedimentary microfacies at J = 87.

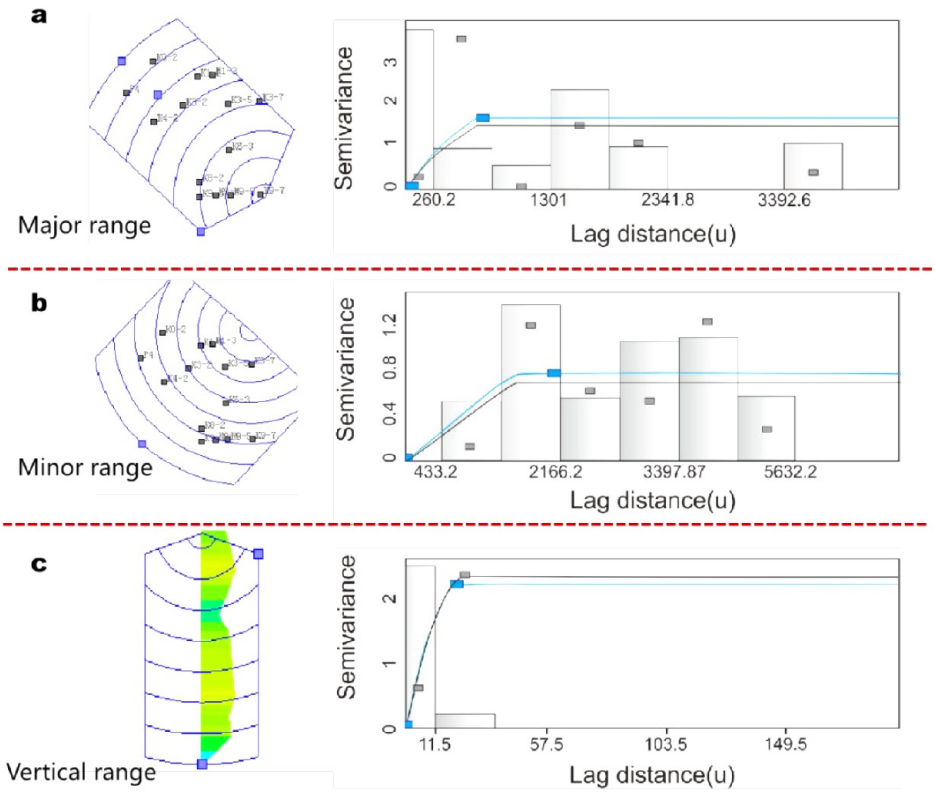

Figure 10. Variogram model of meandering river course sediment control. (Note: left part of a, b, and c - search core of major, minor and vertical; right part of a, b, and c - variogram of each direction; gray quadrilateral in variogram - actual semivariance data; blue quadrilateral in variogram - fitting variogram data).

On the basis of the abundant field outcrop observations and sedimentary geological development practices, the distribution of sedimentary facies indicates its intrinsic rules. A certain genetic relationship is reflected by stratigraphic division and sedimentary models. Sequence stratigraphic division demonstrates a better understanding of the dynamic mechanism of

https://doi.org/10.1021/acsomega.2c01387
ACS Omega 2022, 7, 18004−18016

Table 2. Variogram Parameters Controlled by Different Sedimentary Microfacies

sedimentary microfacies	variogram				
	horizontal range (major)	horizontal range (minor)	vertical range	azimuth (deg)	type
main course	1215.8	536.4	8.7	321	spherical
point bar	1025.4	815.2	9.5	332	spherical
flood fan	807.4	445.7	4.3	335	spherical
natural levee	865.45	775.4	3.7	357	spherical
flood plain	1124.5	787.2	2.1	330	spherical

controlling sediments, and the sedimentary model reflects the genetic relationship between different sedimentary facies and within certain sedimentary facies. Therefore, the model established by sedimentary facies and sequence stratigraphy should better reflect reality than the model established by mathematical statistical well point data.

Because of the hydrodynamic differences between sedimentary environments, the grain size, component morphology, and contact relationship of detrital particles vary; thus, the porosities of sand bodies in various sedimentary facies zones also vary. The application of pure geostatistics or the "one-step modeling method" offers a certain advantage for the heterogeneity of attribute distribution in an underground space. However, the use of pure mathematical or statistical methods to solve geological problems is often akin to "guessing" through a "mathematical game"; these methods cannot combine geological understanding with 3D visualization and digitization. Thus, facies-controlled modeling, a two-step modeling method, is applied to establish the model. First, the sedimentary facies model is established. Second, according to the sandstone porosity distribution law under the control of different sedimentary facies (sand body), the interwell attributes are discretized in the model to establish the facies-controlled porosity model, which is also the groundwater accumulation area model.

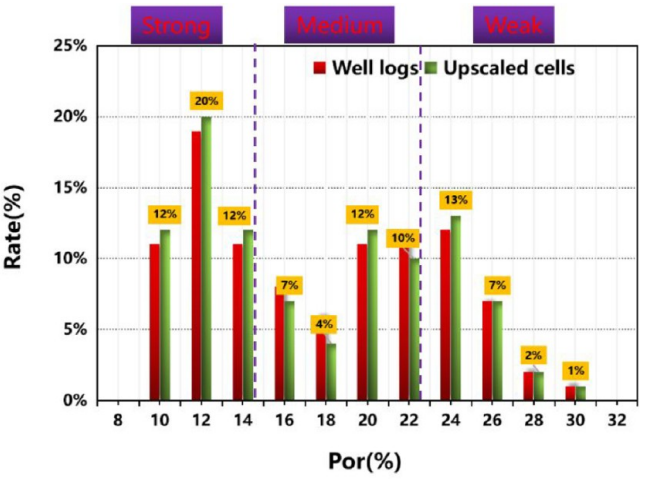

Figure 12. Statistical histogram of well log porosity and upscaled cell porosity.

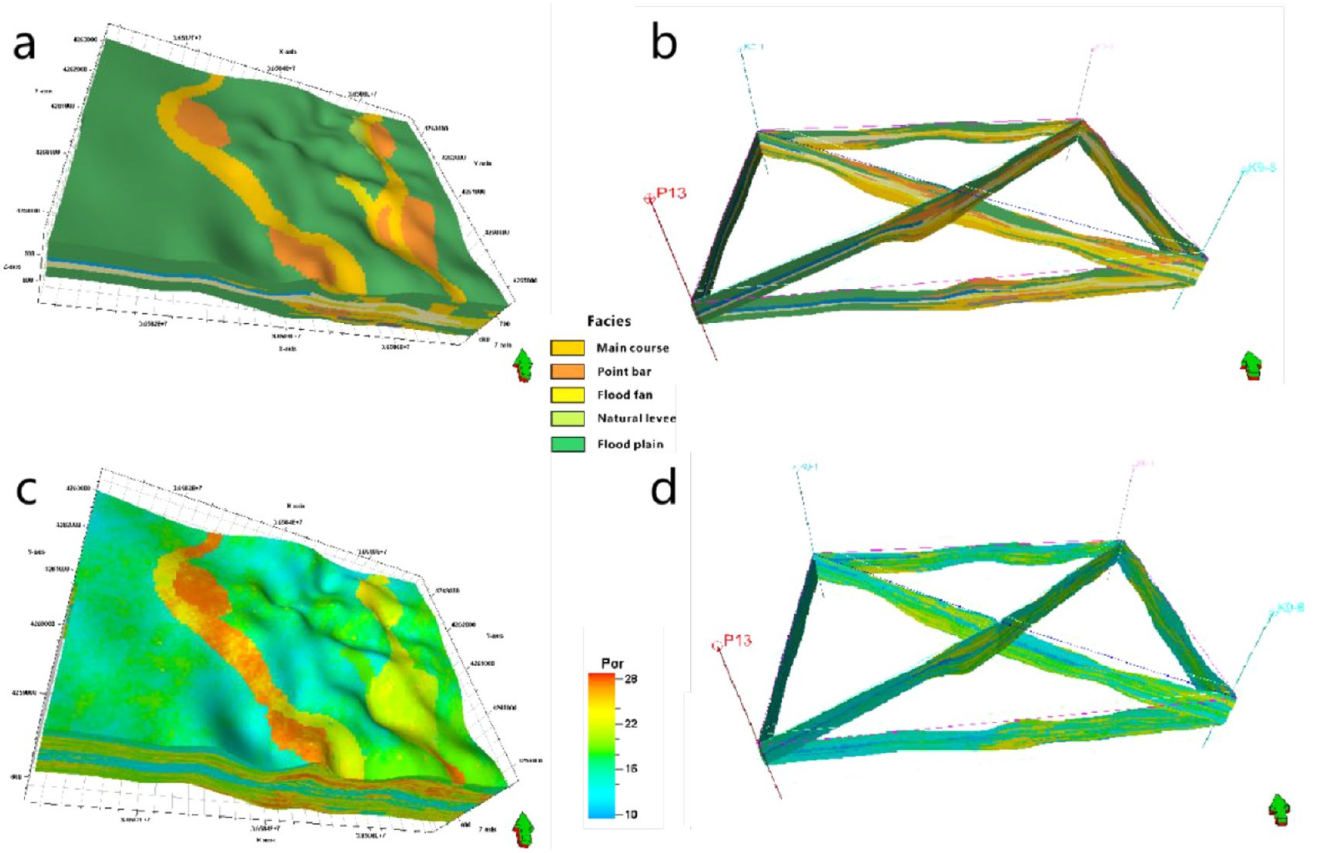

Figure 11. Sedimentary microfacies model and facies-controlled porosity model: (a) sedimentary microfacies model; (b) 3D grid diagram of sedimentary microfacies; (c) 3D porosity model; (d) 3D grid diagram of porosity

https://doi.org/10.1021/acsomega.2c01387
ACS Omega 2022, 7, 18004−18016

Table 3. Comparison of Predicted Results of Facies-Controlled Groundwater Potential in the Study Area

no.	depth (m)	pumping horizon	q (L/s·m)	K (m/d)	sedimentary facies (3D model)	mean predicted porosity (%) (3D model)	predicted result (3D model)
K9-7	625−681	J_2z_{1-2} (625.1−635.4);	0.11441	0.261	flood plain	18.87	moderate
		J_2z_{1-1} (635.4−681)			braided channel		
K1-7	614−703.5	J_2z_{1-2} (624.4−649.4);	0.00466	0.018	flood plain	13.58	weak
		J_2z_{1-1} (649.4−696.5)					
K8-1	645−682	J_2z_{1-1} (648.7−667.5);	0.127	0.212	braided channel	22.57	strong
		J_2y (667.5−682)					
K4-7	590−658	J_2z_{2-2} (584.4−616.8);	0.1514	0.225	estuary dam	19.34	moderate
		J_2z_{2-1} (616.6−652.4)					
K6-2	617.5−660.8	J_2z_{2-2} (617.5−624.8);	0.0941	0.198	delta sand beach	20.54	strong
		J_2z_{2-1} (624.8−654.3)			underwater channel		
K3-4	510.5−600.5	J_2z_{3-2} (498.5−530);	0.1815	0.182	flood plain	16.54	moderate
		J_2z_{3-1} (530−564.3);			flood fan		
		J_2z_{2-2} (560.3−603.4)			estuary dam		
K6-3	510.4−572.4	J_2z_{3-2} (527.3−557.5);	0.0086	0.057	flood plain	11.93	weak
		J_2z_{3-1} (557.5−572.4)			natural levee		

Although the structure is simple and there is almost no fault development in the coalfield of the Ordos Basin, mine water inrush accidents still frequently occur. Moreover, the flow direction of groundwater is also ill-defined in the in situ leaching of uranium. The fundamental reason is that the distribution and accumulation of groundwater is unclear. However, the establishment of a facies-controlled heterogeneous porosity model can solve this problem. Accurate positioning of the groundwater potential area provides a better understanding of the heterogeneity and anisotropy of a coal-measure aquifer, which is of great significance to the layout of a coal mine work surface and the design of water drainage projects for the safe production of coal mines. In addition, many coal-measure aquifers also include uranium ore deposits in the Ordos Basin; thus, the coexploitation of coal and uranium has become necessary.

In summary, the facies-controlled modeling method involves a combination of certainty and randomness. The method not only preserves the heterogeneity of attribute parameters in the stratum but also reflects geological understanding, providing geological guarantees for coal mine- and sandstone-type uranium ore.

3.5.3. Expectations of a 3D-Distributed Model of Chemical Elements in Uranium ore. Uranium in situ leaching is a comprehensive uranium mining and metallurgy technology based on hydrology, geology, and chemistry. A stable weak permeable roof, high porosity and permeability, and appropriate geochemical composition are the three key points of in situ leaching. The leaching agent reacts chemically with the ore in this process, and Ca^{2+}, Fe^{2+}, Fe^{3+}, Mg^{2+}, and other components in the ore are filtered out, forming flocculent or massive precipitation, such as gypsum ($CaSO_4$) and calcite ($CaCO_3$). This precipitation blocks the flow channel of groundwater and reduces the efficiency of in situ leaching uranium mining.

Thus, a 3D distributed model of chemical elements in uranium ore is necessary for in situ leaching. Two key points of element distributed modeling are identified. First, the relationship between the locations of different metallogenic belts and the chemical compositions of ores is significant for in situ leaching because it takes considerable material and financial resources to test the chemical composition of ores. Second, based on geostatistical modeling theories such as truncated Gaussian and sequential indicator simulation, a modified algorithm suitable for the 3D spatial distribution model of chemical elements is necessary.

4. CONCLUSION

A set of established methods for 3D groundwater potential prediction models was developed in this research. Based on data from logging and cores and laboratory experiments, under the control of truncated Gaussian simulation and facies-controlled modeling, a final model was built to predict the groundwater potential area in the Ordos Basin, China. The specific conclusions are as follows:

(1) Different sedimentary microfacies which are affected by sandstone distribution were identified by sedimentary analysis. Because of differences in sedimentary genesis, the shape and amplitude of the logging curve and core are quite different in various sediments at the same time.

(2) The lithoelectric relationship of the Zhiluo Formation in the target area was established. As a result, the porosity of the untested well section was calculated and analyzed. The statistical results show that mud-dominated sediments have relatively poor effective porosity; however, sand-dominated sediments indicate relatively good effective porosity.

(3) The porosity parameters after modeling, indicating strong heterogeneity and large differences in the plane and space, were controlled by the distribution of sedimentary microfacies. According to the principle of natural fracture point

https://doi.org/10.1021/acsomega.2c01387
ACS Omega 2022, 7, 18004−18016

classification, the groundwater potential area was divided into three grades: weak, moderate, and strong.

(4) The validation results indicate that sedimentary areas, such as channels, delta front bars, and estuary bars, have high specific yields, and the groundwater potential is relatively strong; however, the specific yields in flood plains, natural levees, and other mud-dominated sedimentary areas are small, and the groundwater potential is weak. The specific field (actual data), sedimentary microfacies, and predicted porosity of the 3D model showed good correlations, which means that the predicted model of the groundwater potential area is valid.

AUTHOR INFORMATION

Corresponding Author

Fei Xia − *State Key Laboratory of Nuclear Resources and Environment, East China University of Technology, Nanchang 330000, China;* orcid.org/0000-0002-9253-8216; Email: 1400036276@qq.com

Authors

Liyao Li − *State Key Laboratory of Nuclear Resources and Environment and Key Laboratory for Digital Land and Resources of Jiangxi Province, East China University of Technology, Nanchang 330000, China;* orcid.org/0000-0002-0178-1529

Jinhui Liu − *College of Water Resource and Environmental Engineering, East China University of Technology, Nanchang 330000, China*

Kai Zang − *Shandong Institute of Geophysical and Geochemical Exploration, Shandong Provincial Bureau of Geology and Mineral Resources, Jinan 250013, China*

Chao Liu − *Tianjin Branch of CNOOC Limited, Tianjin 300452, China*

Jiuchuan Wei − *College of Earth Science and Engineering, Shandong University of Science and Technology, Qingdao 266000, China*

Longlong Liu − *School of Geographical Sciences, Lingnan Normal University, Zhanjiang 524048, China*

Complete contact information is available at: https://pubs.acs.org/10.1021/acsomega.2c01387

Notes

The authors declare no competing financial interest.

ACKNOWLEDGMENTS

This research was financially supported by the National Natural Science Foundation of China (Grant Nos. 41862010, 42172098, 42102161, and U1967209), Natural Science Foundation of Jiangxi Province (Youth Fund project, No. 20212BAB213006) Opening Fund of the State Key Laboratory of Nuclear Resources and Environment (No. 2020NRE20), and Key Laboratory for Digital Land and Resources of Jiangxi Province (No. DLLJ202108).

REFERENCES

(1) Yin, H.; Shi, Y.; Niu, H.; Xie, D.; Wei, J.; Lefticariu, L.; Xu, S. A GIS-based model of potential groundwater yield zonation for a sandstone aquifer in the Juye Coalfield, Shangdong, China. *J. Hydrol.* **2018**, *557*, 434−447.

(2) Shi, L. Q.; Xu, D. J.; Wang, Y.; Qiu, M. A novel conceptual model of fracture evolution patterns in the overlying strata during horizontal coal seam mining. *Arab J. Geosci.* **2019**, *12* (10), 1−9.

(3) Gao, B.; Sun, Z. X. Applying fluid inclusions to study of metallogensis for sandstone-type uranium deposits in Ordos basin. *Program with Abstracts of the First Meeting Asia Current Research on Fluid Inclusion* **2006**, 88−89.

(4) Shi, S. Q.; Wei, J. C.; Xie, D. L.; Yin, H. Y.; Li, L. Y. Prediction analysis model for groundwater potential based on set pair analysis of a confined aquifer overlying a mining area. *Arab J. Geosci* **2019**, DOI: 10.1007/s12517-019-4267-6.

(5) Gao, W. F.; Shi, L. Q.; Han, J.; Zhai, P. H. Study on control water of Ordovician aquifer, a coal mine of Feicheng mining area, China. *Carbonates Evaporites* **2020**, *35*, 48.

(6) Wu, Q.; Huang, Y. Indications of sandstone-type uranium mineralization from 3D seismic data: a case study of the Qiharigetu deposit, Erenhot Basin, China. *J. Petrol Explor Prod Technol.* **2021**, *11*, 1069−1080.

(7) Wu, Q.; Liu, Y.; Liu, D.; Zhou, W. Prediction of floor water inrush, the application of GIS-based AHP vulnerable index method to Donghuantuo coal mine, China. *Rock Mech Rock Eng.* **2011**, *44*, 591−600.

(8) Gao, W. F.; Shi, L. Q.; Han, J.; Zhai, P. H. Dynamic monitoring of water in a working face floor using 2D electrical resistivity tomography (ERT). *Mine Water Environ.* **2018**, *37* (3), 423−430.

(9) Zhou, C. C.; Wang, Y. J.; Zhou, F. M. Modeling and application of the lithofacies-controlled primary pore reservoir of proximal sandstone. *Pet Explor Dev.* **2006**, *33* (5), 553−557.

(10) Haldorsen, H. H.; Damsleth, E. Stochastic modeling. *J. Pet. Technol.* **1990**, *42*, 404−412.

(11) Lee, S. Y.; Carle, S. F.; Fogg, G. E. Geologic heterogeneity and a comparison of two geostatistical models: Sequential Gaussian and transition probability-based geostatistical simulation. *Adv. Water Resour.* **2007**, *30*, 1914−1932.

(12) Verly, G. W. *Sequential Gaussian Cosimulation: A Simulation Method Integrating Several Types of Information Geostatistics Troia 92*; Springer: Netherlands,.1993; pp 543−554.

(13) Yi, C.; Wang, G.; Li, P.; Zhang, Y.; Luo, X. N. The Relationship between Alteration Characteristics and Uranium Mineralization in Zhiluo Formation, North-Eastern Ordos Basin. *Acta Geol Sin-engl.* **2019**, *93* (z2), 130−131.

(14) Li, L. Y. Research on 3D architecture modeling of facies-controlled aquifer and water abundance mechanism-take Yingpanhao coal mine in Dongsheng coalfield as an example. Doctoral dissertation. Shandong University of Science and Technology, 2019.

(15) Zhang, R. *Fluid-rock interaction and reservoir effects of sandstones in the central Ordos Basin*; Liaoning Science and Technology Press (in Chinese), 2017.

(16) Smith, R.; Møllern, N. Sedimentology and reservoir modeling of the Ormen Lange field, mid Norway. *Mar Pet Geol.* **2003**, *20*, 601−613.

(17) Deutsch, C. V.,. *Geostatistical reservoir modeling*. Oxford University Press, New York. 2002.

(18) Xu, X. T.; Zhao, M. N.; Deng, A.; Wang, S. S. A Study on the Measurement and Classification of Rural Construction Land Consolidation Potential. *Urbanization and Intensive Land Use* **2018**, *6* (4), 77−82.

(19) Chen, A. Q.; Zhang, X. X.; Mi, W. T.; Kang, Y. M.; Liu, Y. C.; Wang, L. G.; Du, J. N.; Hou, M. C.; Liao, Z. L. Characteristics of the middle Jurassic Zhiluo Formation reservoir sand body and its accumulation model in the southwest of Ordos Basin. *J. Earth Sci. Environ.* **2019**, *41* (05), 517−528 (in Chinese with English abstract)..

(20) Emery, X.; Cornejo, J. Truncated Gaussian simulation of discrete-valued, ordinal coregionalized variables. *Comput. Geosci-UK.* **2010**, *36* (10), 1325−1338.

(21) Xing, X. J.; Liu, Y. Q.; Li, W. H.; Gong, B. L.; Xing, X. J.; Liu, Y. Q.; Li, W. H.; Gong, B. L. Sandstone diagenesis and uranium mineralization of the Zhiluo formation in the Diantou area, southern Ordos Basin. *Acta Geol Sin-engl.* **2008**, *29* (2), 179−188.

(22) Li, L. Y.; Qu, J.; Wei, J. C.; Xia, F.; Gao, J. D.; Liu, C. Facies-Controlled Geostatistical Porosity Model for Estimation of the

Groundwater Potential Area in Hongliu Coalmine, Ordos Basin, China. *ACS Omega.* **2021**, *6* (15), 10013−10029.
(23) Naghibi, S. A.; Pourghasemi, H. R. A comparative assessment between three machine learning models and their performance comparison by bivariate and multivariate statistical methods in groundwater potential mapping. *Water Resour Manag.* **2015**, *29*, 5217−5236.
(24) Ma, D.; Zhang, J.; Duan, H.; Huang, Y.; Zhou, N. Reutilization of gangue wastes in underground backfilling mining: overburden aquifer protection. *Chemosphere* **2021**, *264* (Pt 1), 128400.
(25) Ma, D.; Duan, H.; Liu, W.; Ma, X.; Tao, M. Water−sediment two-phase flow inrush hazard in rock fractures of overburden strata during coal mining. *Mine Water and the Environment* **2020**, *39*, 308.
(26) Ma, D.; Duan, H.; Zhang, J.; Feng, X.; Huang, Y. Experimental investigation of creep-erosion coupling mechanical properties of water inrush hazards in fault fracture rock masses. *Chinese Journal of Rock Mechanics and Engineering* **2021**, *40* (09), 1751−1763 (in Chinese with English abstract)..

https://doi.org/10.1021/acsomega.2c01387
ACS Omega 2022, 7, 18004−18016